



Preparation and employment of carbon nanodots to improve electron extraction capacity of polyethylenimine interfacial layer for polymer solar cells



Xinyuan Zhang ^a, Zhiqi Li ^a, Zhihui Zhang ^a, Chunyu Liu ^a, Jinfeng Li ^a, Wenbin Guo ^{a,*}, Liang Shen ^a, Songnan Qu ^{b,**}

^a State Key Laboratory on Integrated Optoelectronics, College of Electronic Science and Engineering, Jilin University, 2699 Qianjin Street, Changchun 130012, China

^b State Key Laboratory of Luminescence and Applications, Changchun Institute of Optics, Fine Mechanics and Physics, Chinese Academy of Sciences, 3888 Eastern South Lake Road, Changchun 130033, China

ARTICLE INFO

Article history:

Received 24 December 2015

Received in revised form

28 February 2016

Accepted 5 March 2016

Available online 15 March 2016

Keywords:

Carbon nanodots

Polymer solar cells

Electron extraction capacity

Charge mobility

ABSTRACT

The performance of polymer solar cells is substantially enhanced by introducing carbon nanodots as additives in polyethylenimine buffer layer. The most pronounced effect is observed in one type of device with the average power conversion efficiencies increased from 5.78% to 7.56% after the addition of carbon nanodots at an optimal concentration in the interfacial layer, which is mainly attributed to the enhanced light trapping and electron transfer in the devices. Besides the light-harvesting and electron transport capacity improvement, the addition of carbon nanodots can also increase exciton generation and dissociation, leading to a high electron mobility. This study demonstrates a facile approach for enhancing the efficiencies of polymer solar cells.

© 2016 Elsevier B.V. All rights reserved.

1. Introduction

As an emerging photovoltaic technology, polymer solar cells (PSCs), which are based on polymer:fullerene composites with a bulk heterojunction (BHJ) structure and solution-processed process, have become a highlight research area in view of their immense potential as promising alternatives for renewable energy generation in recent years [1–3]. One of the most concerned and critical issues of PSCs for commercialization is the power conversion efficiency (PCE) of the devices [4–11]. However, the efficiency of PSCs is not sufficient to meet realistic specifications for widespread commercialization compared with their inorganic counterparts. Recently, many strategies have been employed to improve the PCEs of PSCs based on different principles, such as introduction of buffer layers, additives, noble metal nanoparticles with plasmonic effects, tandem structure, etc. The continuous improvements in device efficiency have been made and PCEs of PSCs have

dramatically increased from about 2.5% to exceeding 10% [11–19].

One limitation of many high-efficiency PSCs is the low electron mobility in the devices, which prohibit the further improvement of the device performance [20–24]. For BHJ PSCs, excitons excited by light absorption need to diffuse at the donor/acceptor interface and dissociate into free charges. Highly efficient PSCs require maximizing charge transport efficiencies and minimizing charge carrier recombination losses. Whereas, there exists a trade-off between the sweep-out of the free charges by the built-in potential and recombination of the free charges due to the low mobility of polymer semiconductors [25,26]. Furthermore, it is still a bottleneck that the optical absorption can be improved by increasing the thickness of active layer, while thicker films usually cause higher charges recombination and larger device resistance, which limits the increase of short-circuit density (J_{sc}) and fill factor (FF). Considerable efforts have been taken to tackle this issue through the design of narrow bandgap donor-conjugated polymers, the invention of novel device structures, the electrode interfacial engineering, and the optimization of processing techniques via proper additives [27–34]. Among them, an effective and convenient approach for pursuing high PCE is to incorporate quantum dots

* Corresponding author.

** Corresponding author.

E-mail addresses: guowb@jlu.edu.cn (W. Guo), qusn@ciomp.ac.cn (S. Qu).

(QDs) material into devices, such as directly patterning on the interfaces of anode and cathode, doping into active layers or both [35–38]. As we know, good electrical properties for solar cells such as a low series resistance and a high shunt resistance, which are associated with the contact at photoactive layer/electrodes (superior diode quality) and good bulk conductivity of the device, are responsible for the device efficiency enhancement. Especially, the electrode interface engineering aims at improving the electrical contact between active layer and electrode, which is conducive to efficient charge extraction, so that electrons and holes are selected and transformed from active layer to their respective electrodes [39–42]. Recently, amine-rich polyethylenimine (PEI) has been applied as a hole-blocking layer for PSCs and a high device efficiency has been achieved [43,44]. It is cost-effective, stable in aqueous solutions, environment friendly, and suitable for a solution process at low temperature. However, pristine PEI polymer is insulating with low conductivity and produces a high resistance in a thick film, which usually restricts the photocurrent of PSCs.

In this work, carbon nanodots (Cdots) were incorporated into PEI buffer layer of inverted PSCs based on poly [N-9'-hepta-decanoyl-2,7-carbazolealt-5,5-(4',7'-di-2-thienyl-2',1',3'-benzothiadiazole)] (PCDTBT):fullerene derivative [6,6]-phenyl-C₇₁-butyric acid methyl ester (PC₇₁BM) to form a high performance cathode interfacial layer for realizing a cell with high efficiency and better stability. Cdots is a good additive to PEI due its good solubility in water, good conductivity, and good film-forming properties. Compared to pristine PEI as the electron transport layer, the PEI modified with Cdots resulted in remarkably increased J_{sc}, FF, and PCE.

2. Experimental section

2.1. Carbon dots preparation and property

The microwave synthesis of Cdots follows procedures given in our previous work [45]. Citric acid (3 g) and urea (6 g) were added to distilled water (20 ml) to form a transparent solution. The solution was then heated in a domestic 650 W microwave oven for 4–5 min, during which the solution changed from being a colorless liquid to a brown and finally dark-brown clustered solid, indicating the formation of Cdots. This solid was then transferred to a vacuum oven and heated at 60 °C for 1 h. A sample of the Cdots was diluted in aqueous solution, which was purified in a centrifuge (10000 r/min, 20 min) to remove large or aggregated particles.

The morphologies of Cdots were characterized using transmission electron microscopy (TEM). Drops of Cdots dilute aqueous solution were deposited on carbon-coated copper grids for TEM. Morphology characterizations illustrated that Cdots are spherical

and well dispersed (Fig.1(a)). The sizes of Cdots were in the range from 1 to 5 nm. Well-resolved lattice fringes with an interlinear spacing of 0.32 nm of Cdots (Fig.1(b)) are close to the (002) facet of graphitic carbon. The Cdots dilute aqueous solution exhibits excitation-wavelength-dependent PL (Fig.2(a)). The strongest emission was observed centered at 540 nm under 420-nm excitation with PL quantum yield of 18%. The maximum absorption band of Cdots aqueous solution was observed at 420 nm, indicating π-π conjugated structure (Fig.2(b)). The surface functional groups of Cdots were detected using Fourier transform infrared (FT-IR) (Fig.2(c)). Broad absorption bands at 3050–3552 cm⁻¹ are assigned to ν(N-H) and ν(O-H). Absorption bands at 1640–1780 cm⁻¹ are assigned to ν(C=O). The absorption band centered at 1566 cm⁻¹ is assigned to C=N bond. These functional groups improve hydrophilicity and stability of the prepared Cdots in aqueous systems.

2.2. Device fabrication and characterization

The Cdots material was dissolved in deionized water and the concentration was 2 mg/mL. The chemical structure of PEI, PCDTBT, PC₇₁BM are shown in Fig.3(a), and Fig.3(b) are schematic device structure and energy levels. The device structure is glass/indium tin oxide(ITO) (150 nm)/PEI:Cdots(10 nm)/PCDTBT: PC₇₁BM (100 nm)/molybdenum oxide (MoO₃) (4 nm)/silver (Ag) (100 nm). The preparation of devices is described in the following script. Firstly, ITO-coated glass substrates were cleaned in an ultrasonic bath with detergent, acetone, isopropyl alcohol, and deionized water and then dried under a N₂ stream. Then, the substrates were treated using a UV/O₃ photoreactor to eliminate surface contaminants for 10 min. For the electron-transport layer, PEI was dissolved in deionized water (2 mg/mL). Meanwhile, various additive amounts of 0, 0.5 μL, 1 μL, 2 μL, 3 μL, and 4 μL Cdots solution were mixed into each 1 mL PEI solution, and corresponding weight ratios (wt.) of Cdots and PEI are 0, 0.5 wt.%, 1.0 wt.%, 2.0 wt.%, 3.0 wt.%, and 4.0 wt.%, respectively. The devices made with different additive concentrations of Cdots were named as Device A, Device B, Device C, Device D, Device E, and Device F. The blend solutions were ultrasonic treated for 30 min, then spin-coated at 4000 rpm on top of the ITO in air. In our experiments, 4000 rpm is the optimal parameter obtained through a large number of trials. The thin film was then heated to 100 °C and kept in glove box for 10 min. For active layer, the 1,2-dichlorobenzene (DCB) solution composed of PCDTBT (7 mg/mL) and PC₇₁BM (28 mg/mL) were spin-cast at 2000 rpm on top of the PEI layer in air subsequently. The fabricated chips with active layer were baked in the atmosphere of argon in the glove box at 70 °C for 20 min. Finally, the cells were fabricated by thermal evaporation of 4 nm MoO₃ and 100 nm Ag as electrode. MoO₃ possessing the highest occupied molecular orbital (HOMO)

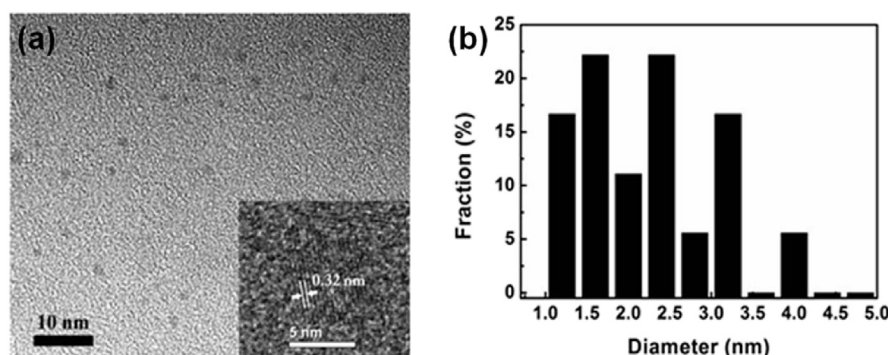


Fig. 1. (a) TEM image of Cdots deposited from water solution on a carbon-coated copper grid, (b) the corresponding size distributions of Cdots in TEM observations.

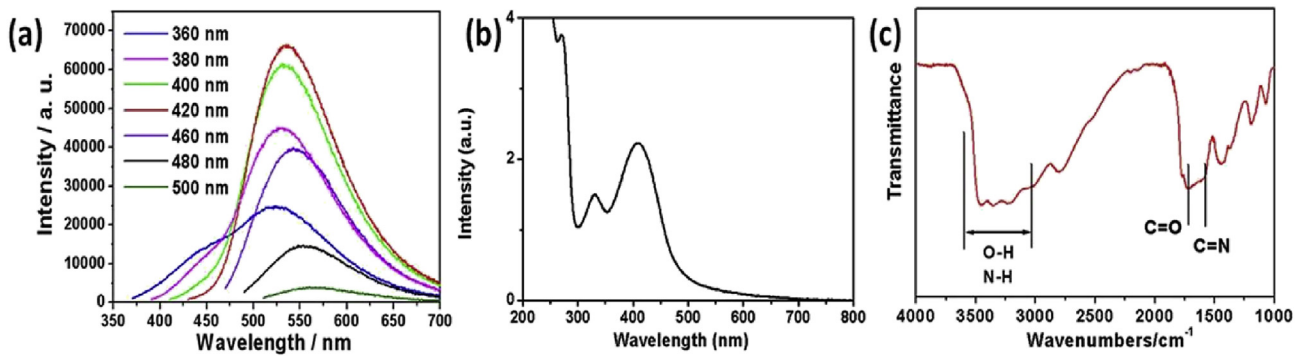


Fig. 2. (a) PL spectra of Cdots dilute aqueous solution at different excitation wavelengths, (b) UV–Vis absorption spectra of Cdots dilute aqueous solutions, (c) FT-IR spectra of Cdots in the dry state.

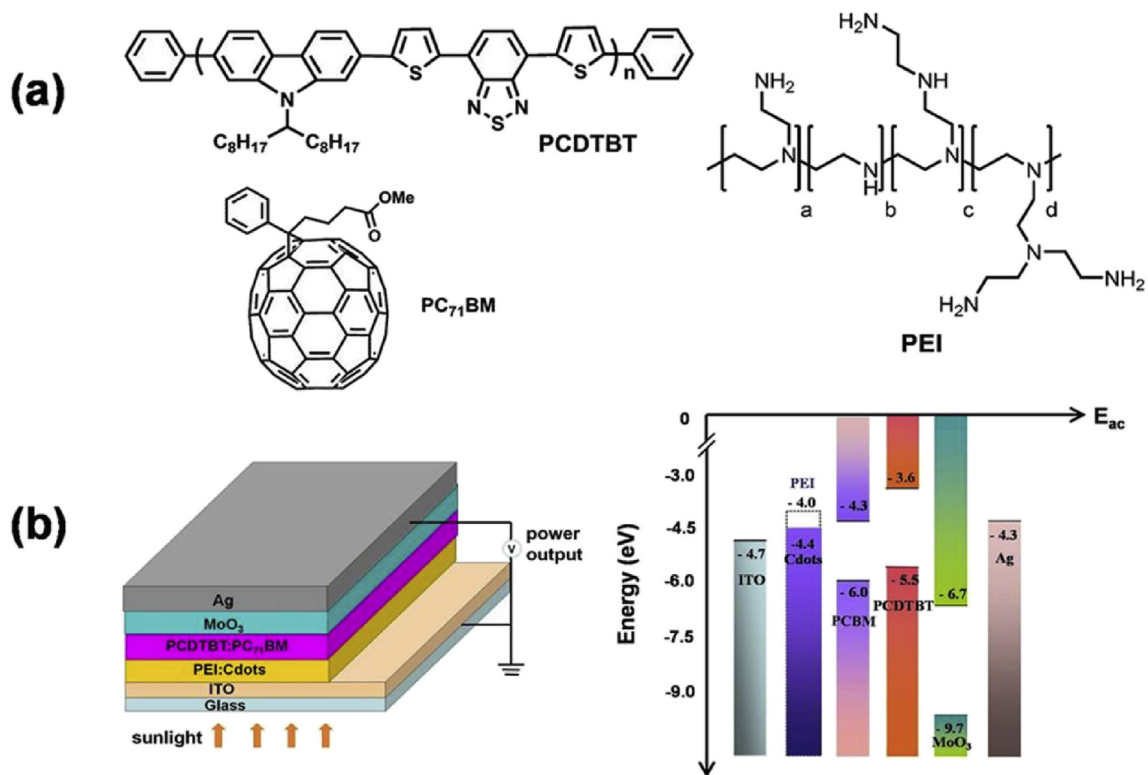


Fig. 3. (a) Chemical structure of materials involved in this study, (b) the device structure and scheme of energy levels of the inverted polymer solar cells.

level of -9.7 eV was selected as a hole transport layer at the photoactive layer interface due to its ability of enhancing hole collection [46–48]. The active area of the device was about 6.4 mm^2 . Current density-voltage (J-V) characteristics of the finished devices were measured using a computer-programmed Keithley 2601 source/meter under AM1.5G solar illuminations with an Oriel 300 W solar simulator intensity of $\sim 100\text{ mW cm}^{-2}$ (about one sun) in air without encapsulation. The light intensity was measured with a photometer (Internationallight, IL1400) corrected by a standard silicon solar cell. The incident photon-to-current efficiency (IPCE) was measured with CrowntechQTest Station 1000 AD.

3. Results and discussion

To investigate the effect of Cdots additive on the morphology of the different interfacial layers, we measured the typical atomic

force microscopy (AFM) morphology images of pristine PEI, 1.0 wt.% Cdots modified PEI, and 4.0 wt.% Cdots modified PEI, respectively, and results were shown in Fig. 4. The root-mean-square (RMS) roughness of three films were 1.03 nm (Fig. 4(a)), 2.71 nm (Fig. 4(b)), and 3.32 nm (Fig. 4(c)), respectively. The morphology of PEI film with 1.0 wt.% Cdots shows a higher roughness than pristine PEI, which extends the interfacial contact area between the buffer layer and active layer, which is beneficial to electron collection by thin PEI film modified ITO. The PEI film with 4.0 wt.% Cdots additive shows a remarkable molecular aggregation due to the excess Cdots, which may have negative effect on the continuity of the film, resulting in a higher charge recombination probability.

The J-V characteristics of the devices with different concentrations of Cdots under an intensity of 100 mW/cm^2 in ambient air are illustrated in Fig. 5(a). The control device with PEI layer exhibits an average J_{sc} of 13.79 mA/cm^2 , an average V_{oc} of 0.84 V , and a FF of

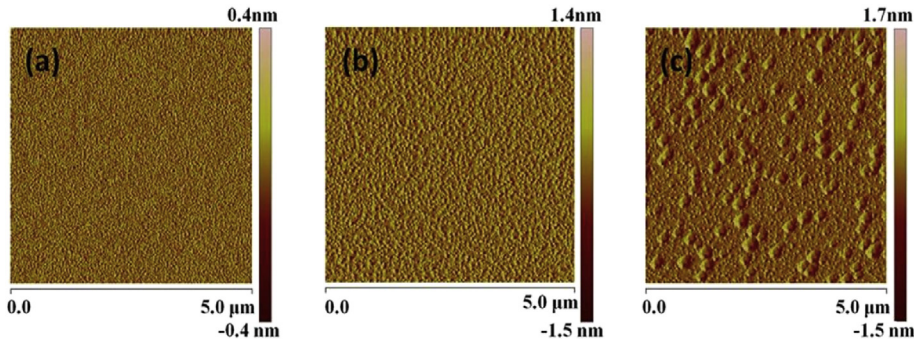


Fig. 4. AFM morphology image of (a) pristine PEI, (b) 1.0 wt.% Cdots modified PEI, and (c) 4.0 wt.% Cdots modified PEI.

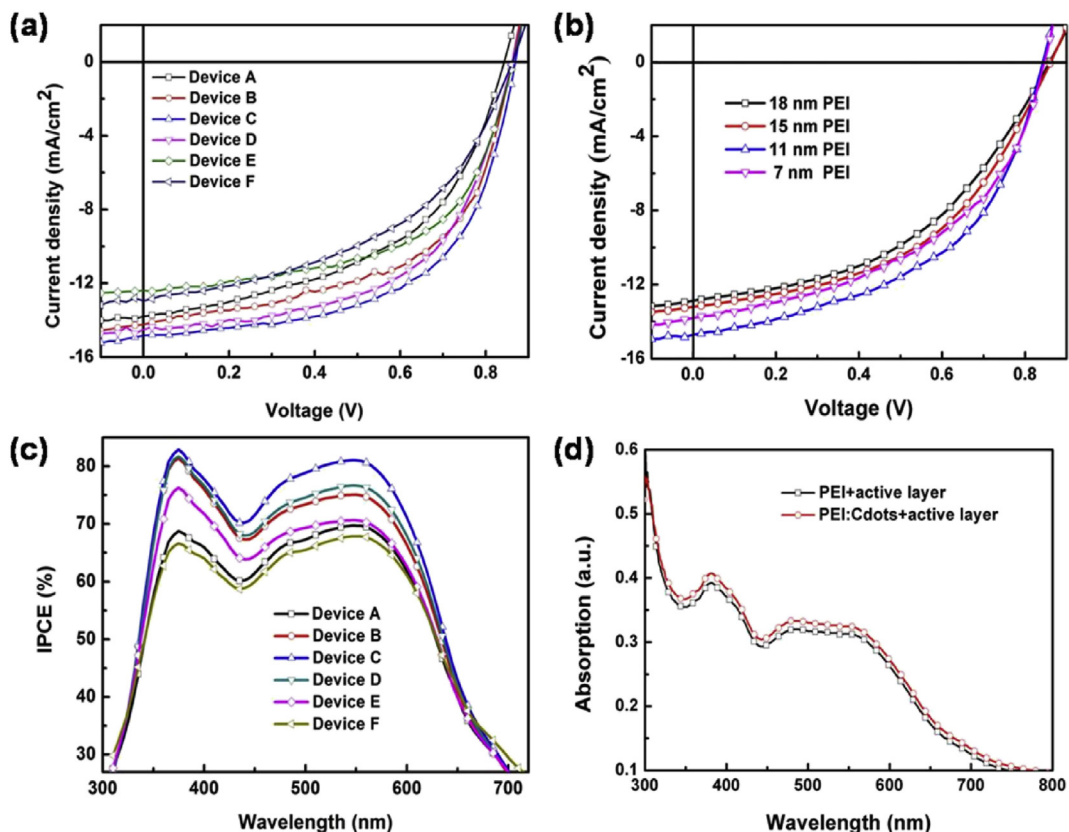


Fig. 5. (a) The J–V characteristics of all devices without and with various concentrations of Cdots in PEI layer, (b) J–V characteristics of PSCs with various thickness of pristine PEI buffer layer, (c) IPCE spectra of cells without and with various concentrations of Cdots, (d) the absorption spectra including active layer with pristine PEI and optimized PEI:Cdots films.

49.88%, leading to a PCE of 5.78%. And we also fabricated a reference device based on Cdots film as electron transporting layer, which owns a J_{sc} of 12.96 mA/cm², a V_{oc} of 0.72 V, a FF of 48.2%, leading to a PCE of 4.5%. After adding Cdots into PEI buffer layer, the cells performance was remarkably improved. The PCE of Device C made with an optimal Cdots of 1.0 wt.% is 7.56%, with a J_{sc} of 14.84 mA/cm², a V_{oc} of 0.87 V, and a FF of 58.54%. Also, the V_{oc} of Device C had a slightly increase compared to the control device. Furthermore, J_{sc} and FF are both improved dramatically, and it is observed that J_{sc} rises from 13.79 mA/cm² to 14.84 mA/cm² and FF increases from 49.88% to 58.54%, which directly leads to a PCE enhancement of 30.79% than control device. Meanwhile, Device B, Device D, Device E, and Device F were also conducted, the detailed parameters including V_{oc} , J_{sc} , FF, and PCE of all fabricated devices are

summarized in **Table 1**, and each value is typical average of 30 devices. It is worthy noting that V_{oc} of all modified devices have a slightly enhancement compared with control device. With the increase of additive concentration, J_{sc} , FF and PCE of modified devices have conspicuous change trend, and they rise first and then decrease with the increase of Cdots. Device B, D and E demonstrate relatively higher PCEs than control device, therein they exhibit PCEs of 6.86%, 7.02%, and 6.06%, respectively. PEI layer incorporated with Cdots possesses an advantage to improve electron transport and reduce charge recombination, which reduces the space charge buildup affecting the internal field in the case of control device, leading to an increase of FF. Furthermore, the introducing of Cdots into PEI cathode buffer layer slightly enhanced light absorption, which contributes to the increase of photon-generated carriers.

Table 1

The key photovoltaic parameters, including short-circuit current density (J_{sc}), open-circuit voltage (V_{oc}), power conversion efficiency (PCE), fill factor (FF), series resistance (R_s), and shunt resistance (R_{sh}) based on different concentrations Cdots additive.

Device	V_{oc} (V)	J_{sc} (mA cm $^{-2}$)	FF(%)	PCE(%)	R_s (ohm)	R_{sh} (ohm)
A	0.84 ± 0.01	13.79 ± 0.12	49.88 ± 0.02	5.78 ± 0.14	172.82	3312.89
B	0.87 ± 0.01	14.24 ± 0.11	55.35 ± 0.01	6.86 ± 0.12	132.83	3700.09
C	0.87 ± 0.01	14.84 ± 0.19	58.54 ± 0.03	7.56 ± 0.20	99.73	13836.51
D	0.86 ± 0.01	14.51 ± 0.14	56.26 ± 0.04	7.02 ± 0.12	138.52	25679.91
E	0.86 ± 0.01	12.39 ± 0.08	56.85 ± 0.02	6.06 ± 0.14	141.56	9573.79
F	0.86 ± 0.01	12.34 ± 0.11	47.17 ± 0.01	5.01 ± 0.13	229.27	11381.55

Series resistance (R_s) and shunt resistance (R_{sh}) of modified and control devices were also estimated and compared, which are also included in Table 1. Apparently, it can be seen that R_s defined by the slope of the J-V curve decreases from 172.82 to 99.73 Ω for Device A and Device C, but R_{sh} of modified devices is significantly increased. The R_s decrease and R_{sh} increase are both advantageous for the FF improvement [49–53]. We also found that Device F produced a negative effect, which implied that excess additive damaged charge transport capacity of PEI buffer layer. In addition, we also measured J-V characteristics of PSCs with various thickness of pristine PEI as electron transport layer (Fig.5(b)). The thickness of PEI layer is altered by rpm of spin-coating (2000 rpm, 3000 rpm, 4000 rpm, 5000 rpm), and the corresponding thickness of PEI film are 18 ± 1 nm, 15 ± 1 nm, 11 ± 1 nm, and 7 ± 1 nm, respectively. It can be seen from Fig.5(b) that the device with 11 nm PEI layer exhibits the best PCE, and the PCEs of the devices with PEI layer is slightly lower than that of devices with PEI:Cdots buffer layer. The incident photon-to-current efficiency (IPCE) spectra of all fabricated devices are shown in Fig.5(c). Device C with 1.0 wt.% Cdots shows the maximum IPCE of about 80% around 400 nm, which is much higher than the control device. All these results are consistent with the J-V characteristic shown in Fig.5(a) and provide a direct evidence for the enhancement of J_{sc} . After modified with Cdots, the IPCEs significantly increase covering a broad photoresponse of wavelength range from 350 to 750 nm. This result is agreement with the absorption spectrum of PEI/PCDTBT:PC₇₁BM films without and with 1.0 wt.% Cdots (Fig.5(d)).

The light absorption improvement of the composite film modified with Cdots (Fig.5(d)) could be caused by a range of reasons, including scattering from the rougher surface, shadowing, parasitic absorption of Cdots, different film formation of PEI film with Cdots. To verify the effect of Cdots on light harvesting, we measured the absorption spectrum of PEI film, PEI:Cdots (1.0 wt.%) film, PEI/PCDTBT:PC71BM film, and PEI:Cdots(1.0 wt.%)/PCDTBT:PC71BM film, respectively. The net light absorption of PCDTBT:PC₇₁BM films on PEI and PEI:Cdots were deduced and

shown in Fig.6(a), which indicates that the light harvesting of active layer on PEI:Cdots layer is a little higher than that on PEI layer. The incident light energy into the device can be divided four parts, which are absorption, transmittance, reflection and scattering (including other effect such as shadowing). Therefore, in order to further explore the action mechanism of Cdots on light trapping of active layer, we tested the light absorption, transmittance, and reflection of PEI and PEI:Cdots films, respectively. The light absorption, transmittance, and reflection were subtracted from the total incident light, the rest of light energy can be ascribed to scattering and other effect. Fig.6(b) is the scattering and other optical effect spectrum of PEI and PEI:Cdots films, and the higher scattering effect of PEI:Cdots film contributes to the light absorption of active layer. Moreover, the peak of Cdots photoluminescence (PL) spectra (Fig.2(a)) occurs in the region of 450 to 650 nm, which locates in the range of the absorption spectra of active layer. Overlap of the absorption spectra of active layer and PL spectra of Cdots is beneficial to the light utilization [54].

In order to investigate the effect of Cdots on the electron extraction property, a single-electron device was fabricated, whose configuration is ITO/PEI:Cdots/active layer/Bathocuproine (BCP)/Ag, and the BCP is hole blocking layer (Fig.7(a)). The electron mobility in the blend film can be determined from current-voltage measurements by using electrodes to suppress the injection of holes. Electron mobility was estimated using the space-charge-limited current (SCLC) model, including field dependence [55]. At a typical applied voltage of 1.0 V, corresponding to an electric field of 10^5 V cm $^{-1}$ across the bulk of a 100 nm device, electron mobility increases from 2.7×10^{-3} to 5.5×10^{-3} cm 2 V $^{-1}$ s $^{-1}$ for Device A and Device C. Obviously, the electron mobility in the PEI:Cdots is a little higher than that in the PEI film due to the electric conductivity improvement, allowing to better charge extraction from active layer, which renders electrons effectively transport to cathode electrode. The dark J-V characteristics of all devices were shown in Fig.7(b), and it can be seen that the dark J_{sc} apparently increased after Cdots introducing. Meanwhile, the largest J_{sc} value with the

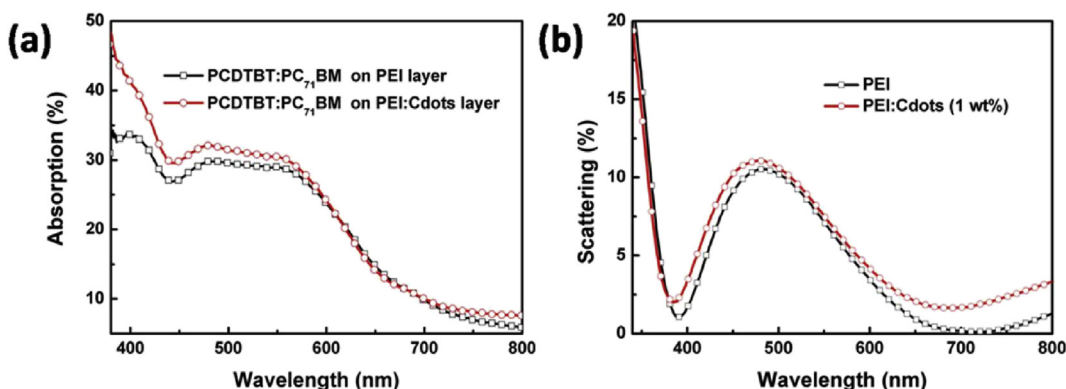


Fig. 6. (a) the light absorption of active layers on PEI and PEI:Cdots (1.0 wt.%) layers, (b) the scattering and other optical effect occurring in PEI and PEI:Cdots (1.0 wt.%) layers.

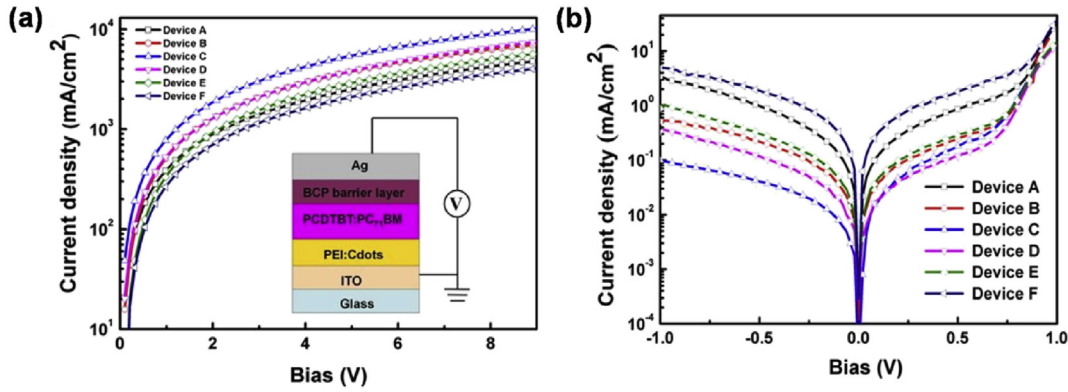


Fig. 7. (a) J-V characteristics of electron-only devices in dark with the device structure inset, (b) J-V characteristics of devices without and with different amounts of Cdots in dark.

additive concentration of 1.0 wt.% was obtained, which is consistent with the tendency of the photocurrent in Fig.5(a). Additionally, the dark J_{sc} of modified devices have been enhanced irrespective of additive concentrations due to enhancement of electron mobility by incorporating Cdots. The current density of devices is suppressed in the region between -1.0 and 1.0 V. Except for Device F, all the modified devices show smaller leakage current at negative voltages in the case of the incorporation of Cdots, and the enhanced dark J-V characteristics is also reflected by FF. To directly explore the electron transfer mechanism in Cdots modified device, the changes in the work function (WF) induced by Cdots were measured using a Kelvin probe system (KP 6500 Digital Kelvinprobe, McAllister Technical Services Co., Ltd.). We chose the WF of Au (5 eV) as a reference, and the WF of PEI and PEI:Cdots films were characterized by $WF = 5eV - WF_{Au\text{-measure}} + WF_{measure}$. Hence, the work function of PEI and Cdots are -4.0 and -4.4 eV respectively, and the work function of PEI:Cdots is about -4.15 eV [56,57]. The incorporation of Cdots can reduce the work function of PEI film, which decreases energy barrier for electron injection from active layer to PEI and tunes energy level of buffer layer in our cells. The WF tuning provided efficient charge collection center and remarkably accelerated charge transfer rates from excited organic molecules to ITO. In fact, the formation of tight nanoscale domains of PEI:Cdots film improved interfacial contact and reduces the interface resistance. The presence of the Cdots filled the ditch of PEI layer, which decrease interfacial charge trammel and reduce the charge recombination possibility. Meanwhile, Cdots worked as efficient charge collection matrix, which penetrate around the fullerene clusters and the polymer-skin, enhancing diffusion in the process of electron transport. Therefore, cell performance will be energetically favored at the PEI:Cdots layer [58,59].

The incorporation of Cdots also improves the charge collection efficiency under working conditions. Fig.8(a) shows the J-V characteristics in a wide reverse bias range under AM 1.5G illumination. The results are plotted as the net photocurrent ($J_{ph} = J_L - J_D$) dependence on the effective applied voltage V_{eff} ($V_{eff} = V_0 - V_a$). J_L and J_D are the current density under illumination and in the dark, respectively. V_0 is the voltage when J_{ph} equals zero (i.e., $J_L = J_D$), and V_a is the applied voltage [60]. At a large reverse voltage, J_{ph} reaches saturation for all devices, suggesting all photogenerated excitons are dissociated into free charges and all carriers are collected at the electrodes without any bimolecular recombination [61]. In this case, current density J_{sat} is only determined by the amount of absorbed incident photon flux (N_{photon}), thus the maximal obtainable exciton generation rates (G_{max} , given by $J_{sat} = qG_{max}L$ where L is the thickness of the active layer) for the control and optimal modified devices were $1.21 \times 10^{26} \text{ m}^{-3} \text{ s}^{-1}$ ($J_{sat} = 193.67 \text{ Am}^{-2}$) and

$1.42 \times 10^{26} \text{ m}^{-3} \text{ s}^{-1}$ ($J_{sat} = 227.89 \text{ Am}^{-2}$), respectively. Apparently, a noticeable enhancement in G_{max} occurred after incorporating the Cdots into the device. Then we compared the exciton dissociation probabilities [$P(E,T)$] for all devices (Fig.8(b)), which are correlated with the electric field (E) and temperature (T). When the excitons are photogenerated in PSCs, only a part of them can be dissociated into free carriers. As a result, J_{ph} can be expressed using the equation, $J_{ph} = qG_{max}P(E, T)L$, and the value of $P(E,T)$ can be obtained from the plot of the normalized photocurrent density (J_{ph}/J_{sat}) with respect to V_{eff} at any bias [62,63]. Fig.8(b) reveals that the values of $P(E,T)$ under the short-circuit conditions ($V_a = 0$ V) increased from 69.67% for the control device to 77.49% for the optimal modified device. In view of the value of G_{max} is related to maximum absorption, such an increase suggests enhanced light absorption of the active layer for the modified devices. Since the ratio of J_{ph}/J_{sat} is substantially the product of exciton dissociation efficiency and charge collection efficiency, an enhanced J_{ph}/J_{sat} suggests the increased exciton generation rate, the dissociation probability, and charge collection efficiency, which leads to a higher FF for PSCs [64].

To explore the effect of Cdots on the charge transfer property, steady-state photoluminescence (PL) measurements were further performed. Fig.9(a) showed the PL spectra of PEI film without and with Cdots. In general, PL intensity of pristine PEI is higher than PEI with Cdots. The PL spectra showed significant decreasing intensities at about 400 nm and 700 nm with the increase of additive amount. The fluorescence process is positive correlated with photon-generated electrons and holes radiative loss, which is disadvantage to the free charge carriers transport and collected by electrodes. This indicates that more efficient charge transfer occurs in the blend transport layer due to the existence of Cdots than in the pristine PEI film. Attributed to incorporated Cdots into PEI, the fluorescence quenching is decreased, which means photon-generated carriers radiative loss diminished, and more electrons can be injected into cathode. To deeply understand the impact of Cdots in PEI buffer layer on the interface resistance of devices, impedance spectroscopy was measured with an alternating current signal under open circuit voltage in the frequency range of 20 Hz to 20 MHz [65]. Fig.9(b) presents the Cole-Cole curves of the impedance spectra for the devices without and with different concentrations Cdots in dark. At the open circuit voltage condition, the built-in electric field was canceled out by the applied bias voltage, preventing the photogenerated charge carriers in the active layer from flowing toward electrodes. An accurately model was set up according to experimental data that resembles the typical semicircle shape. The shapes of impedance spectra are all semicircles, which are beneficial to investigate the interface resistance for the cells. The series resistance of photovoltaic cells is

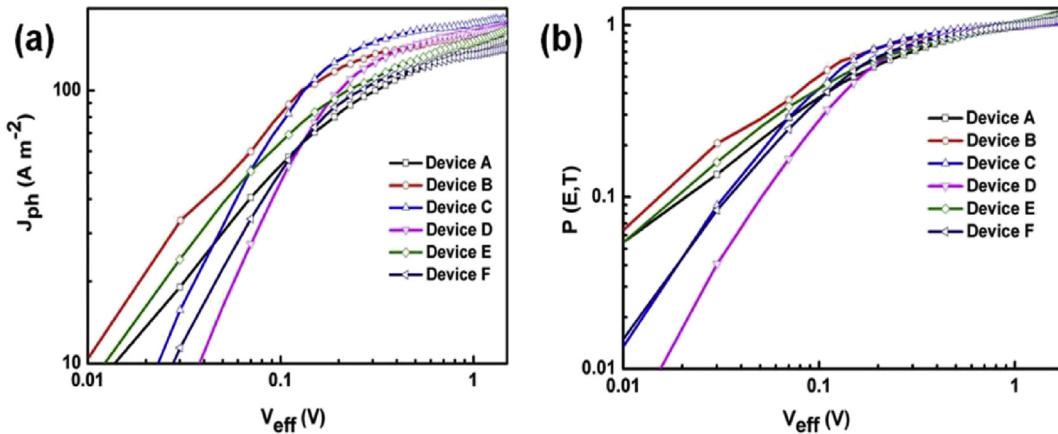


Fig. 8. (a) Plots of photocurrent density (J_{ph}) with respect to the effective voltage (V_{eff}) for control and modified devices under constant incident light intensity, (b) Corresponding plots exciton dissociation probability [$P(E,T)$] with respect to effective bias (V_{eff}) for all cells.

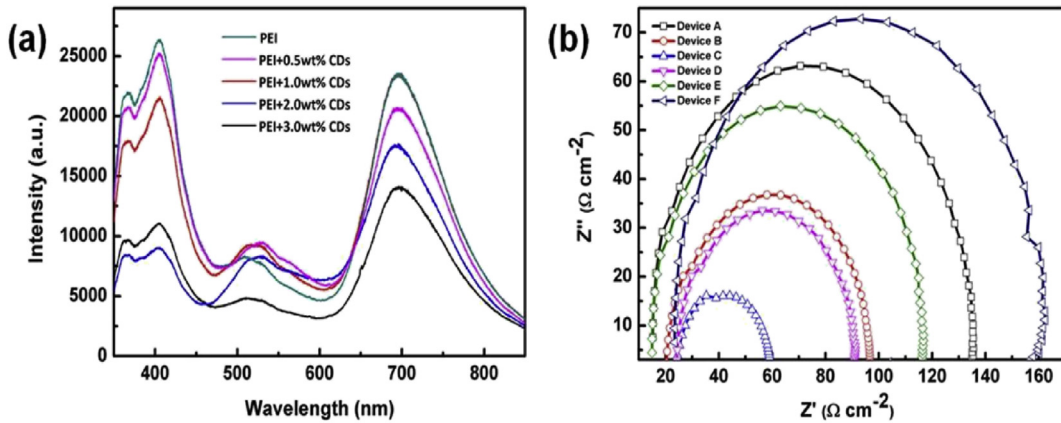


Fig. 9. (a) Photoluminescence (PL) spectra of PEI films modified with different amount of Cdots, (b) the impedance spectra diagram of all devices.

closely related to the diameter of the semicircles. The semicircle's diameter in the diagram stands for the impedance values, and the larger diameter means larger impedance. Therefore, the impedance of devices modified with moderate Cdots is much smaller than control device [66,67]. By incorporating Cdots into PEI layer can extends the interfacial contact area between the buffer layer and active layer, forming a better interface, and thus the injection barrier is decreased. Thus, the introduction of Cdots brings a significant decline to the device impedance, which contributes to the enhancement of FF and PCE. According to the data in Table 1, the series resistance (R_s) of the best modified device is calculated as $99.73 \Omega/\text{cm}^2$, which is smaller than control device. Moreover, the shunt resistance (R_{sh}) of all modified devices increases by more than an order of magnitude compared with control device. These data are in agreement with the decreased leakage current and slightly increased V_{oc} in the devices, which indicated that better diode characteristics were achieved after simple incorporating Cdots into PEI layer.

4. Conclusion

In summary, we have demonstrated that remarkable enhancement of short-circuit current density and fill factor can be achieved in highly efficient polymer solar cells by simply introducing Carbon nanodots in PEI buffer layer, resulting in a PCE up to 7.56%. For the optimal additive concentration, the J_{sc} , FF, and PCE are 7.61%, 17.36%,

and 30.79% higher than the control cells, respectively. The effects of Cdots incorporating on the improvement of device performance are threefold: an improved built-in potential across the device due to the existence of interface dipole, improved charge-transport properties, and decreased recombination loss due to the increase of charge carrier mobility. The approach reported here provides a simple and versatile method to optimize polymer solar cells and may set the efficiency of devices towards the goal of 10% from popular material systems.

Acknowledgments

The authors are grateful to National Natural Science Foundation of China (61275035, 61370046, 11574110), Project of Science and Technology Development Plan of Jilin Province (20130206075SF, 20140101060JC, 20150519003JH), Key Technology Research and Development Program of Changchun (13KG66), the Opened Fund of the State Key Laboratory on Integrated Optoelectronics (IOSKL2013KF10), Project of Graduate Innovation Fund of Jilin University (2015098) for the support to the work.

References

- [1] X.C. Li, F.X. Xie, S.Q. Zhang, J.H. Hou, W.C.H. Choy, MoO_x and V₂O_x as hole and electron transport layers through functionalized intercalation in normal and inverted organic optoelectronic devices, *Light Sci. Appl.* 4 (2015) e273.
- [2] T.D. Nielsen, C. Cruickshank, S. Foged, J. Thorsen, F.C. Krebs, Market and

- intellectual property analysis of polymer solar cells, *Sol. Energy Mat. Sol. Cells* 94 (2010) 1553–1571.
- [3] C. Edwards, A. Arbabi, G. Popescu, L.L. Goddard, Optically monitoring and controlling nanoscale topography during semiconductor etching, *Light Sci. Appl.* 1 (2012) e30.
- [4] F.C. Krebs, S.A. Gevorgyan, J. Alstrup, A roll-to-roll process to flexible polymer solar cells: model studies, manufacture and operational stability studies, *J. Mat. Chem.* 9 (2009) 5442–5451.
- [5] G. Yu, J. Gao, J.C. Hummelen, F. Wudl, A.J. Heeger, Polymer photovoltaic cells: enhanced efficiencies via a network of internal donor-acceptor heterojunctions, *Science* 270 (1995) 1789–1791.
- [6] C. Edwards, A. Arbabi, G. Popescu, L.L. Goddard, Optically monitoring and controlling canoscale topography during semiconductor etching, *Light Sci. Appl.* 1 (2012) e30.
- [7] C. Tao, S. Ruan, X. Zhang, G. Xie, L. Shen, X. Kong, W. Dong, C. Liu, W. Chen, Performance improvement of inverted polymer solar cells with different top electrodes by introducing a MoO₃ buffer layer, *Appl. Phys. Lett.* 93 (2008) 193307.
- [8] H. Zang, Y. Liang, L. Yu, B. Hu, Intra-molecular donor–acceptor interaction effects on charge dissociation, charge transport, and charge collection in bulk-heterojunction organic solar cells, *Adv. Energy Mater* 1 (2011) 923–929.
- [9] G. Dennler, M.C. Scharber, C.J. Brabec, Polymer-fullerene bulkheterojunction solar cells, *Adv. Mater* 21 (2009) 1323–1338.
- [10] Y. Kim, S. Cook, S.M. Tuladhar, S.A. Choulis, J. Nelson, J.R. Durrant, D.D.C. Bradley, M. Giles, I. McCulloch, C.S. Ha, M. Ree, A strong regioregularity effect in self-organizing conjugated polymer films and high-efficiency poly-thiophene: fullerene solar cells, *Nat. Mater* 5 (2006) 197–203.
- [11] B.C. Park, S.H. Yun, C.Y. Cho, Y.C. Kim, J.C. Shin, H.G. Jeon, Y.H. Huh, I.C. Hwang, K.Y. Baik, Y.J. Lee, Surface plasmon excitation in semitransparent inverted polymer photovoltaic devices and their applications as label-free optical sensors, *Light Sci. Appl.* 3 (2014) e222.
- [12] S.E. Shaheen, C.J. Brabec, N.S. Sariciftci, F. Padinger, T. Fromherz, J.C. Hummelen, 2.5% efficient organic plastic solar cells, *Appl. Phys. Lett.* 78 (2001) 841–843.
- [13] Z.C. He, C.M. Zhong, X. Huang, W.Y. Wong, H.B. Wu, L.W. Chen, S.J. Su, Y. Cao, Simultaneous enhancement of open-circuit voltage, short-circuit current density, and fill factor in polymer solar cells, *Adv. Mater* 23 (2011) 4636–4643.
- [14] C.E. Small, S. Chen, J. Subbiah, C.M. Amb, S.W. Tsang, T.H. Lai, J.R. Reynolds, F. So, High-efficiency inverted dithienogermole–thienopyrrolodione-based polymer solar cells, *Nat. Phot.* 6 (2012) 115–120.
- [15] L.T. Dou, J.B. You, J. Yang, C.C. Chen, Y.J. He, S. Murase, T. Moriarty, K. Emery, G. Li, Y. Yang, Tandem polymer solar cells featuring a spectrally matched low-bandgap polymer, *Nat. Phot.* 6 (2012) 180–185.
- [16] Z.C. He, C.M. Zhong, S.J. Su, M. Xu, H.B. Wu, Y. Cao, Enhanced power-conversion efficiency in polymer solar cells using an inverted device structure, *Nat. Phot.* 6 (2012) 591–595.
- [17] X.H. Li, W.C.H. Choy, L.J. Huo, F. Xie, W.E.I. Sha, B.F. Ding, X. Guo, Y.F. Li, J.H. Hou, J.B. You, Y. Yang, Dual plasmonic nanostructures for high performance inverted organic solar cells, *Adv. Mater* 24 (2012) 3046–3052.
- [18] J.B. You, L.T. Dou, K. Yoshimura, T. Kato, K. Ohya, T. Moriarty, K. Emery, C.C. Chen, J. Gao, G. Li, Y. Yang, A polymer tandem solar cell with 10.6% power conversion efficiency, *Nat. Commun.* 4 (2013) 1446.
- [19] L.T. Dou, W.H. Chang, J. Gao, C.C. Chen, J.B. You, Y. Yang, A selenium-substituted low-bandgap polymer with versatile photovoltaic applications, *Adv. Mater* 25 (2013) 825–831.
- [20] C.J. Brabec, A. Cravino, D. Meissner, N.S. Sariciftci, T. Fromherz, M.T. Rispens, L. Sanchez, J.C. Hummelen, Origin of the open circuit voltage of plastic solar cells, *Adv. Funct. Mater* 11 (2001) 374–380.
- [21] C.J. Brabec, S.E. Shaheen, C. Winder, N.S. Sariciftci, Effect of LiF/metal electrodes on the performance of plastic solar cells, *Appl. Phys. Lett.* 80 (2002) 1288–1290.
- [22] H. Frohne, S.E. Shaheen, C.J. Brabec, D.C. Muller, N.S. Sariciftci, K. Meerholz, Influence of the anodic work function on the performance of organic solar cells, *J. Chem. Phys. Chem.* 3 (2002) 795–799.
- [23] C.M. Ramsdale, J.A. Barker, A.C. Arias, J.D. MacKenzie, R.H. Friend, N.C. Greenham, The origin of the open-circuit voltage in polyfluorene-based photovoltaic devices, *Appl. Phys.* 92 (2002) 4266–4270.
- [24] V.D. Mihaileti, P.W.M. Blom, J.C. Hummelen, M.T. Rispens, Cathode dependence of the open-circuit voltage of polymer:fullerene bulk heterojunction solar cells, *J. Appl. Phys.* 94 (2003) 6849–6855.
- [25] D.H. Wang, D.Y. Kim, K.W. Choi, J.H. Seo, S.H. Im, J.H. Park, O.O. Park, A.J. Heeger, Enhancement of donor-acceptor polymer bulk heterojunction solar cell power conversion efficiencies by addition of Au nanoparticles, *Angew. Chem. Int. Ed.* 50 (2011) 5519–5523.
- [26] M.M. Mandoc, W. Veurman, L.J.A. Koster, B. De Boer, P.W.M. Blom, Origin of the reduced fill factor and photocurrent in MDMO-PPV: PCNEPV all-polymer solar cells, *Adv. Funct. Mater* 17 (2007) 2167–2173.
- [27] R.A. Taylor, T. Otanicar, G. Rosengarten, Nanofluid-based optical filter optimization for PV/T systems, *Light Sci. Appl.* 1 (2012) e34.
- [28] C. Xiang, W. Koo, F. So, H. Sasabe, J. Kido, A systematic study on efficiency enhancements in phosphorescent green, red and blue microcavity organic light emitting devices, *Light Sci. Appl.* 2 (2013) e74.
- [29] H.Q. Wang, M. Batentschuk, A. Osvet, L. Pinna, C.J. Brabec, Rare-earth ion modified up-conversion materials for photovoltaic applications, *Adv. Mater* 23 (2011) 2675–2680.
- [30] S. Liu, F.X. Meng, W.F. Xie, Z.H. Zhang, L. Shen, C.Y. Liu, Y.Y. He, W.B. Guo, S.P. Ruan, Performance improvement of inverted polymer solar cells by doping Au nanoparticles into TiO₂ cathode buffer layer, *Appl. Phys. Lett.* 103 (2013) 233303.
- [31] C. Chen, F.M. Li, Improving the efficiency of ITO/nc-TiO₂/CdS/P3HT: PCBM/PEDOT: PSS/Ag inverted solar cells by sensitizing TiO₂ nanocrystalline film with chemical bath-deposited CdS quantum dots, *Nanoscale Res. Lett.* 8 (2013) 453.
- [32] F.M. Li, C. Chen, F. Chen, R. Tan, G.T. Yue, L. Shen, W.F. Zhang, A new method to disperse CdS quantum dot-sensitized TiO₂ manotube arrays into P3HT: PCBM layer for the improvement of efficiency of inverted polymer solar cells, *Nanoscale Res. Lett.* 9 (2014) 240.
- [33] D. Chen, A. Nakahara, D. Wei, D. Nordlund, T.P. Russell, P3HT/PCBM bulk heterojunction organic photovoltaics: correlating efficiency and morphology, *Nano Lett.* 11 (2011) 561.
- [34] H. Ma, H.L. Yip, F. Huang, A.K.Y. Jen, Interface engineering for organic electronics, *Adv. Funct. Mater* 20 (2010) 1371–1388.
- [35] X. Chen, B.H. Jia, Y.A. Zhang, M. Gu, Exceeding the limit of plasmonic light trapping in textured screen-printed solar cells using Al nanoparticles and wrinkle-like graphene sheets, *Light Sci. Appl.* 2 (2013) e92.
- [36] Z. Holman, S. Wolf, C. Ballif, Improving metal reflectors by suppressing surface plasmon polaritons: A priori calculation of the internal reflectance of solar cell, *Light Sci. Appl.* 2 (2013) e106.
- [37] P. Cheng, Y. Li, X. Zhan, Efficient ternary blend polymer solar cells with indene-C₆₀ bisadduct as an electron-cascade acceptor, *Energy Environ. Sci.* 2 (2014) 2005–2011.
- [38] S. Honda, T. Nogami, H. Ohkita, H. Benten, S. Ito, Improvement of the light-harvesting efficiency in polymer/fullerene bulk heterojunction solar cells by interfacial dye modification, *ACS Appl. Mat. Interfaces* 1 (2009) 804–810.
- [39] H.L. Yip, A.K.Y. Jen, Recent advances in solution-processed interfacial materials for efficient and stable polymer solar cells, *Energy Environ. Sci.* 5 (2012) 5994–6011.
- [40] Y. Zhu, X. Xu, L. Zhang, J. Chen, Y. Cao, High efficiency inverted polymeric bulk-heterojunction solar cells with hydrophilic conjugated polymers as cathode interlayer on ITO, *Sol. Energy Mat. Sol. Cells* 97 (2012) 83–88.
- [41] L.J. Zuo, X.X. Jiang, M.S. Xu, L.G. Yang, Y.X. Nan, Q.X. Yan, H.Z. Chen, Enhancement of short current density in polymer solar cells with phthalocyanine Tin (IV) dichloride as interfacial layer, *Sol. Energy Mat. Sol. Cells* 95 (2011) 2664–2669.
- [42] C. Edwards, A. Arbabi, G. Popescu, L. Goddard, Optically monitoring and controlling nanoscale topography during semiconductor etching, *Light Sci. Appl.* 1 (2012) e30.
- [43] C.J. Brabec, A. Cravino, D. Meissner, N.S. Sariciftci, T. Fromherz, M.T. Rispens, L. Sanchez, J.C. Hummelen, Origin of the open circuit voltage of plastic solar cells, *Adv. Funct. Mater* 11 (2001) 374–380.
- [44] H. Kang, S. Hong, J. Lee, K. Lee, Electrostatically self-assembled nonconjugated polyelectrolytes as an ideal interfacial layer for inverted polymer solar cells, *Adv. Mater* 24 (2012) 3005–3009.
- [45] S. Qu, X. Liu, X. Guo, M. Chu, L. Zhang, D. Shen, Amplified spontaneous green emission and lasing emission from carbon nanoparticles, *Adv. Funct. Mater* 24 (2014) 2689–2695.
- [46] E.G. Wang, L. Wang, L. Lan, C. Luo, W. Zhuang, J. Peng, Y. Cao, High-performance polymer heterojunction solar cells of a polysilafluorene derivative, *Appl. Phys. Lett.* 92 (2008) 033307.
- [47] Y.J. He, H.Y. Chen, J.H. Hou, Y.F. Li, Indene-C₆₀ bisadduct: a new acceptor for high-performance polymer solar cells, *J. Am. Chem. Soc.* 132 (2010) 1377–1382.
- [48] J. Cremer, P. Bäuerle, M.M. Wienk, R.A.J. Janssen, High open-circuit voltage poly(ethynylene bithiophene):fullerene solar cells, *Chem. Mater* 18 (2006) 5832–5834.
- [49] S. Qu, X. Liu, X. Guo, M. Chu, L. Zhang, D. Shen, Amplified spontaneous green emission and lasing emission from carbon nanoparticles, *Adv. Funct. Mater* 24 (2014) 2689–2695.
- [50] S. Qu, X. Wang, Q. Lu, X. Liu, L. Wang, A biocompatible fluorescent ink based on water-soluble luminescent carbon nanodots, *Angew. Chem. Int. Ed.* 51 (2012) 2215–2218.
- [51] Y. Zhou, C. Fuentes-Hernandez, J. Shim, J. Meyer, A.J. Giordano, H. Li, P. Winget, T. Cheun, H. Papadopoulos, J. Kim, A universal method to produce low-work function electrodes for organic electronics, *Science* 336 (2012) 327–332.
- [52] M. Kroger, S. Hamwi, J. Meyer, T. Riedl, W. Kowalsky, A. Kahn, P-type doping of organic wide band gap materials by transition metal oxides: a case-study on molybdenum trioxide, *Org. Electron* 10 (2009) 932–938.
- [53] Y.H. Su, Y.F. Ke, S.L. Cai, Q.Y. Yao, Surface plasmon resonance of layer-by-layer gold nanoparticles induced photoelectric current in environmentally-friendly plasmon-sensitized solar cell, *Light Sci. Appl.* 1 (2012) e14.
- [54] V. Gupta, V. Bharti, M. Kumar, S. Chand, A.J. Heeger, Polymer–polymer Förster resonance energy transfer significantly boosts the power conversion efficiency of bulk-heterojunction solar cells, *Adv. Mater* 27 (2015) 4398–4404.
- [55] D. Lepage, A. Jimenez, J. Beauvais, J.J. Dubowski, Conic hyperspectral dispersion mapping applied to semiconductor plasmonics, *Light Sci. Appl.* 1 (2012) e28.
- [56] C.J. Brabec, V. Dyakonov, J.S. Parisi, N.S. Sariciftci, *Organic Photovoltaics—Concepts and Realization*, Springer, Berlin, 2003.

- [57] H. Ishii, K. Sugiyama, E. Ito, K. Seki, Energy level alignment and interfacial electronic structures at organic/metal and organic/organic interfaces, *Adv. Mater.* 11 (1999), 0806–0605.
- [58] Y. Yao, J. Hou, Z. Xu, G. Li, Y. Yang, Effects of solvent mixtures on the nanoscale phase separation in polymer solar cells, *Adv. Funct. Mater.* 18 (2008) 1783–1789.
- [59] H. Hoppe, N.S. Sariciftci, Morphology of polymer/fullerene bulk heterojunction solar cells, *J. Mat. Chem.* 16 (2006) 45–61.
- [60] W.B. Guo, K.Z. Zheng, W.F. Xie, L. Sun, L. Shen, C.Y. Liu, Y.Y. He, Z.H. Zhang, Efficiency enhancement of inverted polymer solar cells by doping NaYF₄:Yb³⁺, Er³⁺ nanocomposites in PCDTBT: PCBM active layer, *Sol. Energy Mat. Sol. Cells* 124 (2014) 126–132.
- [61] D.H. Wang, D.Y. Kim, K.W.J. Choi, H. Seo, S.H. Im, J.H. Park, O.O. Park, A.J. Heeger, Enhancement of donor–acceptor polymer bulk heterojunction solar cell power conversion efficiencies by addition of Au nanoparticles, *Angew. Chem. Int. Ed.* 50 (2011) 5519–5523.
- [62] D.D.S. Fung, L.F. Qiao, W.C.H. Choy, C.D. Wang, W.E. Sha, I.F.X. Xie, S.L. He, Optical and electrical properties of efficiency enhanced polymer solar cells with Au nanoparticles in a PEDOT–PSS layer, *J. Mat. Chem.* 21 (2011) 16349–16356.
- [63] E.D. Kosten, J.H. Atwater, J. Parsons, A. Polman, H.A. Atwater, Highly efficient GaAs solar cells by limiting light emission angle, *Light Sci. Appl.* 2 (2013) e45.
- [64] C.C.D. Wang, W.C.H. Choy, C. Duan, D.D.S. Fung, W.E.I. Sha, F.X. Xie, F. Huang, Y. Cao, Optical and electrical effects of gold nanoparticles in the active layer of polymersolar cells, *J. Mat. Chem.* 22 (2012) 1206–1211.
- [65] G. Garcia-Belmonte, A. Munar, E.M. Barea, J. Bisquert, I. Ugarte, R. Pacios, Charge carrier mobility and lifetime of organic bulk heterojunctions analyzed by impedance spectroscopy, *Org. Electron.* 9 (2008) 847–851.
- [66] G.H. Kim, H.K. Song, J.Y. Kim, The effect of introducing buffer layer to polymer solar cells on cell efficiency, *Sol. Energy Mat. Sol. Cells* 95 (2011) 1119–1122.
- [67] G. Perrier, R. de Bettignies, S. Berson, N. Lemaitre, S. Guillerez, Impedance spectrometry of optimized standard and inverted P3HT-PCBM organic solar cells, *Sol. Energy Mat. Sol. Cells* 101 (2012) 210–216.